PERGAMON

International Journal of Solids and Structures 39 (2002) 105–125

INTERNATIONAL JOURNAL OF SOLIDS and STRUCTURES

www.elsevier.com/locate/ijsolstr

In-plane stability of arches

Y.-L. Pi, M.A. Bradford *, B. Uy

School of Civil and Environmental Engineering, The University of New South Wales, Sydney, NSW 2052, Australia

Received 10 December 2000; in revised form 31 July 2001

Abstract

Classical buckling theory is mostly used to investigate the in-plane stability of arches, which assumes that the pre-buckling behaviour is linear and that the effects of pre-buckling deformations on buckling can be ignored. However, the behaviour of shallow arches becomes non-linear and the deformations are substantial prior to buckling, so that their effects on the buckling of shallow arches need to be considered. Classical buckling theory which does not consider these effects cannot correctly predict the in-plane buckling load of shallow arches. This paper investigates the in-plane buckling of circular arches with an arbitrary cross-section and subjected to a radial load uniformly distributed around the arch axis. An energy method is used to establish both non-linear equilibrium equations and buckling equilibrium equations for shallow arches. Analytical solutions for the in-plane buckling loads of shallow arches subjected to this loading regime are obtained. Approximations to the symmetric buckling of shallow arches and formulae for the in-plane anti-symmetric bifurcation buckling load of non-shallow arches are proposed, and criteria that define shallow and non-shallow arches are also stated. Comparisons with finite element results demonstrate that the solutions and indeed approximations are accurate, and that classical buckling theory can correctly predict the in-plane anti-symmetric bifurcation buckling load of non-shallow arches, but overestimates the in-plane anti-symmetric bifurcation buckling load of shallow arches significantly.

Keywords: Analysis; Anti-symmetric; Arches; Bifurcation; Buckling; Instability; Non-linear; Shallow; Snap through; Symmetric

1. Introduction

When the lateral displacements and twist rotations of an arch are fully restrained, the arch (Fig. 1) may buckle in an in-plane anti-symmetric bifurcation mode (Fig. 2(a)) or in an in-plane symmetric snap-through mode (Fig. 2(b)) under in-plane loading (Fig. 1(b)). In order to prevent an arch from in-plane failure, it is important to be able to predict accurately its in-plane elastic buckling load that is needed in the design (Guide to stability design criteria for metal structures, 1988; AS4100, 1998; BS5950, 1998; Load and resistance factor design specification, 1993; Pi and Trahair, 1999). This paper addresses the issue of in-plane elastic stability in shallow and non-shallow arches.

* Corresponding author. Tel.: +61-2-9385-5014; fax: +61-2-9385-6139.
E-mail address: m.bradford@unsw.edu.au (M.A. Bradford).

0020-7683/01/$ - see front matter
PII: S0020-7683(01)00209-8

Nomenclature

A	area of cross-section
A_1, A_2, A_3, A_4	coefficients
B	width of cross-section or flange width of I-section
B_1, B_2, B_3, B_4	coefficients
C, C_1, C_2, C_3, C_4	coefficients
D	overall height of cross-section
D_3, D_4	coefficients
E	Young's modulus of elasticity
f	rise of arch
I_x	second moment of area of cross-section about the major principal axis
k	coefficient
N	$= qR$, nominal axial compression
$\overline{N}$	actual axial compression
N_{F}	classical anti-symmetric buckling load of fixed arches
N_{F1}	classical anti-symmetric buckling load of fixed arches
N_{FB}	classical anti-symmetric buckling load of fixed columns
N_{P}	classical anti-symmetric buckling load of pin-ended arches
N_{P1}	classical anti-symmetric buckling load of pin-ended arches
N_{sb}	$= q_{\mathrm{sb}}R$, nominal anti-symmetric buckling load
N_{ss}	$= q_{\mathrm{ss}}R$, nominal symmetric buckling load
$\bar{q}$	$= (qR - \overline{N})/\overline{N}$, dimensionless measure of the difference between the actual and nominal axial compressions
Q_{s}	axial stress resultant during buckling
q_{sb}	anti-symmetric bifurcation buckling load
q_{ss}	symmetric snap-through buckling load
R	initial radius of arches
r_x	$= \sqrt{I_x/A}$, gyration radius of cross-section about the major principal axis
S	developed length of arch
s, y	coordinates around the arch centre line and toward the arch centre
t	wall-thickness of cross-section
t_{f}	wall-thickness of flange of I-section
t_{w}	wall-thickness of web of I-section
U^*	dimensionless total strain energy
V^*	dimensionless total potential
v	radial displacement
$\tilde{v} = v/R$	dimensionless radial displacement
v_{c}	central radial displacement
$\tilde{v}_{\mathrm{c}} = v_{\mathrm{c}}/R$	dimensionless central radial displacement
$\tilde{v}_{\mathrm{b}}$	dimensionless radial buckling displacement
W^*	dimensionless potential energy of loading
w	axial displacement
$\tilde{w} = w/R$	dimensionless axial displacement
$\tilde{w}_{\mathrm{b}}$	axial buckling displacement
ϵ_{b}	bending strain
ϵ_{m}	membrane strain

ϵ_{mb}	buckling membrane strain
ϵ_P	strain at a point P
λ_s	modified slenderness for in-plane buckling of an arch
μ	$= \sqrt{\overline{N}R^2/EI_x}$
Θ	half of the included angle of an arch
θ	angular coordinate
$(\ )_b$	$\delta(\ )$
$\delta(\ )$	variation of the variable $(\ )$
$(\ )'$	$d(\ )/d\theta$
$(\ )''$	$d^2(\ )/d\theta^2$

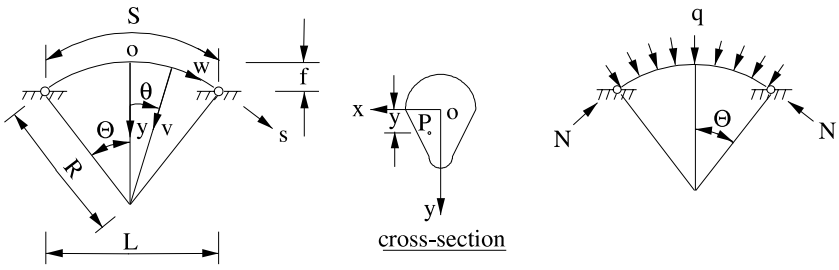

(a) Geometry and cross-section (b) Radial load uniformly distributed around arch

Fig. 1. Arches and loading.

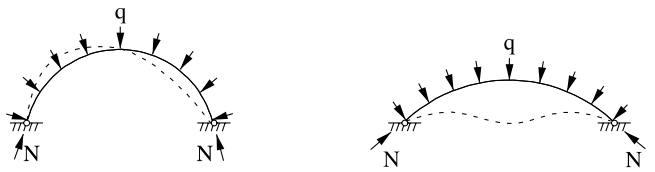

(a) Anti-symmetric bifurcation buckling (b) Symmetric snap-through buckling

Fig. 2. Buckling modes.

So-called classical buckling theory is often used to determine the elastic buckling load of arches (Timoshenko and Gere, 1961; Vlasov, 1961; Simitses, 1976). To facilitate the buckling analysis, some simplifications need to be made in this classical buckling theory (Trahair and Bradford, 1998). Firstly, the pre-buckling behaviour is assumed to be linear so that the stress resultants can be linearised. Secondly, the effects of the pre-buckling displacements on buckling are ignored, while thirdly, the effects of the buckling deformations on the displacement and geometrical stiffnesses are ignored. However, these simplifications may not be valid for shallow arches because the behaviour of shallow arches becomes non-linear and deformations are significant prior to buckling, as pointed out by Pi and Trahair (1998), and so their effects on the in-plane buckling of shallow arches need to be accounted for accurately. These effects may reduce the in-plane buckling resistance of shallow arches significantly, and so classical buckling theory may overestimate the in-plane elastic buckling load of shallow arches.

Early studies on the in-plane buckling of arches are summarised in the Guide to stability design criteria for metal structures (1976, 1988) and the Handbook of structural stability (1971). The buckling of sinusoidal shallow arches was studied by Timoshenko and Gere (1961) and Simitses (1976). Gjelsvik and Bodner (1962) used an energy method to investigate the instability of fixed shallow circular arches with rectangular solid cross-section subjected to central point loading, and approximate solutions were obtained. Schreyer and Masur (1966) performed an exact analysis for shallow circular arches and derived analytical solutions, but their analysis was limited to fixed arches with a rectangular solid section and their solutions for the symmetric buckling mode were very complicated. Dickie and Broughton (1971) used a series method to study the buckling of shallow circular pin-ended and fixed arches. However, their study was also confined again to rectangular solid cross-sections and only approximate numerical solutions were given. In addition to a rectangular section, other shapes such as I-sections and rectangular hollow sections are widely used for arches, as are a number of materials. Although research on the numerical analysis of the buckling of arches has been extensive in recent years (Noor and Peters, 1981; Stolarski and Belytschko, 1982; Calhoun and DaDeppo, 1983; Elias and Chen, 1988; Wen and Suhendro, 1991; Pi and Trahair, 1998), it is not widely recognised that classical buckling theory may overestimate the in-plane buckling load of shallow arches. Because of the lack of analytical solutions for in-plane buckling of shallow arches based on the non-linear theory, analytical solutions based on classical buckling theory may mistakenly be used to verify the effectiveness of finite element results for shallow arches. Using certain finite element codes to obtain the in-plane buckling load of shallow arches is also questionable. Because linear buckling (eigenvalue) analysis is used to obtain the buckling load of a structure in many finite element codes, this method may be erroneously used to obtain the in-plane buckling load of a shallow arch. For example, classical buckling theory has been used to predict the in-plane buckling of shallow arches by some researchers (Rajasekaran and Padmanabhan, 1989; Kang and Yoo, 1994), and these results are at odds with the non-linear analysis presented in the current paper.

The purposes of this paper are threefold: to investigate analytically the elastic in-plane stability of both pin-ended and fixed circular arches with an arbitrary cross-section and subjected to a radial load uniformly distributed around the arch axis; to use an energy method to obtain analytical solutions for the buckling load of the shallow arches including the non-linear effect of pre-buckling deformations; and to propose approximations to the symmetric buckling of the shallow arches and formulas for the in-plane buckling load of both shallow and non-shallow arches.

2. Classical buckling analysis

When an arch is subjected to a radial load q in the direction of the major principal axis of the cross-section and uniformly distributed around the arch axis as shown in Fig. 1, the arch undergoes an uniform axial compression action $N = qR$ where R is the radius of the centroidal axis of the arch. Other conservative distributed loading cases can also be modelled such as hydrostatic pressure (Simitses, 1976; Hodges, 1999) that stays normal to the deformed arch. However, this paper concentrates on the uniformly distributed radial loading case. Classical buckling theory can be used to determine its in-plane buckling load, and this theory is reviewed in the following. In using classical buckling theory, some simplifications need to be made as discussed in the introduction. By using those simplifications and assuming that the major principal axis is directed toward the arch centre, the longitudinal normal strain of an arbitrary point P can be expressed as

$$\epsilon_{\mathrm{P}} = \epsilon_{\mathrm{m}} + \epsilon_{\mathrm{b}} \tag{1}$$

where the membrane strain ϵ_{m} is given by

$$\epsilon_{\mathrm{m}} = \tilde{w}' - \tilde{v} + \tfrac{1}{2}(\tilde{v}' + \tilde{w})^2 \tag{2}$$

and the bending strain ϵ_b is given by (Simitses, 1976; Papangelis and Trahair, 1987)

$$\epsilon_b = -y(\tilde{v}'' + \tilde{w}')/R \tag{3}$$

where $(\ )' = \mathrm{d}(\ )/\mathrm{d}\theta$, $(\ )'' = \mathrm{d}^2(\ )/\mathrm{d}\theta^2$, θ is the angular coordinate, $\tilde{v} = v/R$, $\tilde{w} = w/R$, v and w are the radial and axial displacements respectively, y is the coordinate of the point P in the principal axis system oxy (Fig. 1).

If effects of the membrane strain on the curvature change are considered, the bending strain ϵ_b is then given by (Vlasov, 1961; Pi and Trahair, 1999)

$$\epsilon_b = -y(\tilde{v}'' + \tilde{v})/R \tag{4}$$

Setting the second variation of the total potential of an arch based on the strain of Eqs. (2) and (3) to be equal to zero leads to the energy equation for in-plane buckling of the arch as

$$\frac{1}{2}\int_{-\Theta}^{\Theta}[EA(\tilde{w}_b' - \tilde{v}_b)^2 + EI_x(\tilde{v}_b'' + \tilde{w}_b')^2/R^2 + Q_s(\tilde{v}_b' + \tilde{w}_b)^2]R\,\mathrm{d}\theta = 0 \tag{5}$$

where E is Young's modulus of elasticity, A is the area of the cross-section, I_x is the second moment of the area of the cross-section about its major principal axis, variation of displacements $\delta(\ )$ is written as $(\ )_b = \delta(\ )$, and Q_s is the axial stress resultant given by

$$Q_s = EA(\tilde{w}' - \tilde{v}) = -N \tag{6}$$

The differential equilibrium equations for in-plane buckling can be obtained from the energy equation (5) by use of the calculus of variations, whence upon invoking the Euler–Lagrange equations,

$$[Q_s(\tilde{v}_b' + \tilde{w}_b)]' + EA(\tilde{w}_b' - \tilde{v}_b) - [EI_x(\tilde{v}_b'' + \tilde{w}_b')/R^2]'' = 0 \tag{7}$$

for buckling equilibrium in the radial direction and

$$Q_s(\tilde{v}_b' + \tilde{w}_b) - [EA(\tilde{w}_b' - \tilde{v}_b]' - [EI_x(\tilde{v}_b'' + \tilde{w}_b')/R^2]' = 0 \tag{8}$$

for buckling equilibrium in the axial direction.

If the centre line of the arch is assumed to be inextensible during buckling so that

$$\tilde{w}_b' - \tilde{v}_b = 0 \tag{9}$$

the lowest anti-symmetric buckling load of pin-ended arches can be obtained as (Pi and Bradford, 2000)

$$N_P = \frac{\pi^2 EI_x}{(S/2)^2} \tag{10}$$

while the lowest anti-symmetric buckling load of fixed arches can be obtained as

$$N_F = \frac{(k\pi)^2 EI_x}{(S/2)^2} \tag{11}$$

The value of the parameter k increases with the increase of the included angle 2Θ. When the included angle $2\Theta = 180°$, $k = 1.5$, and when $2\Theta = 0°$, the arch becomes a column and the buckling load (11) becomes that of the second mode of a fixed ended column given by

$$N_{FB} \approx \frac{(1.4303\pi)^2 EI_x}{(S/2)^2} \tag{12}$$

When the strains given in Eqs. (2) and (4) are used, performing the same analysis leads to the lowest buckling load for pin-ended arches as (Pi and Bradford, 2000)

$$N_{\mathrm{P1}} = \frac{[\pi^2 - \Theta^2]EI_x}{(S/2)^2} \tag{13}$$

while the lowest anti-symmetric buckling load of fixed arches can be obtained as

$$N_{\mathrm{F1}} = \frac{[(k\pi)^2 - \Theta^2]EI_x}{(S/2)^2} \tag{14}$$

The value of k increases with the increase of the included angle 2Θ of the arch. When the included angle $2\Theta = 180°$, $k = 1.5$, and when $2\Theta = 0°$, the arch becomes a column and $k \approx 1.4303$.

3. Nonlinear in-plane equilibrium

3.1. Differential equilibrium equations

Because classical buckling theory does not account for the significant effects of pre-buckling deformation and non-linearity on buckling, it cannot be used to predict the in-plane buckling of shallow arches. An energy method is used in this section to investigate the in-plane buckling of shallow arches by accounting for the effects of pre-buckling deformations and geometric non-linearity. The finite element results reported by Pi and Trahair (1998) demonstrated that the axial displacements w of shallow arches are quite small prior to buckling, so that their effects on the radial deformation may be ignored. Thus, the longitudinal normal strain (1) of a point P can further be simplified as

$$\epsilon_{\mathrm{P}} = \epsilon_{\mathrm{m}} + \epsilon_{\mathrm{b}} \tag{15}$$

where the membrane strain ϵ_{m} of Eq. (2) and the bending strain ϵ_{b} of Eqs. (3) or (4) are simplified as

$$\epsilon_{\mathrm{m}} = \tilde{w}' - \tilde{v} + \frac{1}{2}(\tilde{v}')^2 \quad \text{and} \quad \epsilon_{\mathrm{b}} = -\frac{y\tilde{v}''}{R} \tag{16}$$

The total strain energy can be written in a dimensionless form after division by the factor EAR as

$$U^* = \int_{-\Theta}^{\Theta} \frac{1}{2}\left[\epsilon_{\mathrm{m}}^2 + \frac{r_x^2(\tilde{v}'')^2}{R^2}\right] \mathrm{d}\theta \tag{17}$$

where $r_x = \sqrt{I_x/A}$ is the radius of gyration of the cross-section about the major principal axis.

The dimensionless potential energy of the radial load q is

$$W^* = -\int_{-\Theta}^{\Theta} \frac{q\tilde{v}R}{EA} \mathrm{d}\theta \tag{18}$$

The dimensionless total potential of a shallow arch can then be written as

$$V^* = U^* + W^* = \int_{-\Theta}^{\Theta} \left\{ \frac{1}{2}\left[\epsilon_{\mathrm{m}}^2 + \frac{r_x^2(\tilde{v}'')^2}{R^2}\right] - \frac{q\tilde{v}R}{EA} \right\} \mathrm{d}\theta \tag{19}$$

Equilibrium equations can be obtained by invoking Euler–Lagrange equations of variational calculus. For equilibrium in the axial direction,

$$\epsilon_{\mathrm{m}}' = 0 \tag{20}$$

so that the membrane strain ϵ_{m} is a constant and can be written as

$$\epsilon_{\mathrm{m}} = -\frac{\overline{N}}{EA} \tag{21}$$

where $\overline{N}$ is the actual axial compression force in the arch as distinct from its nominal value qR.

For equilibrium in the radial direction,

$$\frac{\tilde{v}^{iv}}{\mu^2} + \tilde{v}'' = \bar{q} \tag{22}$$

where μ is a dimensionless parameter defined by

$$\mu^2 = \frac{\overline{N}R^2}{EI_x} \tag{23}$$

and $\bar{q}$ is a dimensionless load defined by

$$\bar{q} = \frac{qR - \overline{N}}{\overline{N}} \tag{24}$$

which is a measure of the difference between the nominal axial compression qR and the actual axial compression $\overline{N}$.

3.2. Non-linear equilibrium conditions for pin-ended arches

For pin-ended arches, the dimensionless radial displacements $\tilde{v}$, which satisfy the boundary conditions $\tilde{v} = \tilde{v}'' = 0$ at $\theta = \pm\Theta$, can be obtained by solving Eq. (22) as

$$\tilde{v} = \frac{\bar{q}}{\mu^2}\left\{\frac{\cos(\mu\theta) - \cos(\mu\Theta)}{\cos(\mu\Theta)} + \frac{1}{2}[(\mu\theta)^2 - (\mu\Theta)^2]\right\} \tag{25}$$

The non-linear equilibrium conditions for shallow arches can be established by considering that the constant membrane strain given by Eq. (21) should be equal to the average membrane strain over the arch calculated from Eq. (16), so that

$$-\frac{\overline{N}}{EA} = \frac{1}{2\Theta}\int_{-\Theta}^{\Theta}\left(\tilde{w}' - \tilde{v} + \frac{\tilde{v}'^2}{2}\right)\mathrm{d}\theta \tag{26}$$

Using the boundary conditions $\tilde{w} = 0$ at $\theta = \pm\Theta$, it is clear that

$$\frac{1}{2\Theta}\int_{-\Theta}^{\Theta}\tilde{w}'\,\mathrm{d}\theta = 0 \tag{27}$$

and from Eq. (23), the left-hand side of Eq. (26) can be rewritten as

$$-\frac{\overline{N}}{EA} = -\frac{\overline{N}R^2}{EI_x}\frac{1}{R^2}\frac{I_x}{A} = -\frac{\mu^2 r_x^2}{R^2} \tag{28}$$

Considering Eq. (27) and substituting Eqs. (25) and (28) into Eq. (26) leads to the non-linear equilibrium condition for pin-ended shallow arches given by

$$A_1\bar{q}^2 + B_1\bar{q} + C_1 = 0 \tag{29}$$

where

$$A_1 = \frac{1}{4(\mu\Theta)^2}\left[5 - 5\frac{\tan(\mu\Theta)}{\mu\Theta} + \tan^2(\mu\Theta)\right] + \frac{1}{6} \tag{30}$$

$$B_1 = \frac{1}{(\mu\Theta)^2}\left[1 - \frac{\tan(\mu\Theta)}{\mu\Theta}\right] + \frac{1}{3} \tag{31}$$

$$C_1 = \left(\frac{\mu\Theta}{\lambda_s}\right)^2 \tag{32}$$

in which λ_s is the modified slenderness for an arch defined by

$$\lambda_s = \frac{R\Theta^2}{r_x} = \frac{S^2}{4r_x R} \tag{33}$$

3.3. Non-linear equilibrium conditions for fixed arches

For fixed arches, the solution of Eq. (22), which satisfies the boundary conditions $\tilde{v} = \tilde{v}' = 0$ at $\theta = \pm\Theta$, can be similarly obtained as

$$\tilde{v} = \frac{\bar{q}}{\mu^2}\left\{\frac{(\mu\Theta)[\cos(\mu\theta) - \cos(\mu\Theta)]}{\sin(\mu\Theta)} + \frac{1}{2}[(\mu\theta)^2 - (\mu\Theta)^2]\right\} \tag{34}$$

Considering Eq. (27) and substituting Eqs. (28) and (34) into Eq. (26) leads to the non-linear equilibrium condition for fixed arches given by

$$A_2\bar{q}^2 + B_2\bar{q} + C_2 = 0 \tag{35}$$

where

$$A_2 = \frac{5}{12} + \frac{1}{4(\mu\Theta)^2}[3(\mu\Theta)\cot(\mu\Theta) + (\mu\Theta)^2\cot^2(\mu\Theta) - 4] \tag{36}$$

$$B_2 = \frac{1}{3} + \frac{1}{(\mu\Theta)^2}[(\mu\Theta)\cot(\mu\Theta) - 1] \tag{37}$$

$$C_2 = \left(\frac{\mu\Theta}{\lambda_s}\right)^2 \tag{38}$$

4. Buckling analysis

4.1. Buckling equations

The critical condition for buckling may be stated that the second variation of the total potential is equal to zero for any admissible variation of the displacements, which indicates a possible transition from a stable state to an unstable state. Taking the second variation of the dimensionless total potential (19) leads to

$$\frac{1}{2}\delta^2 V^* = \int_{-\Theta}^{\Theta}\frac{1}{2}\left[\left(\epsilon_{mb}^2 + \epsilon_m\tilde{v}_b'^2\right) + \frac{r_x^2\tilde{v}_b''^2}{R^2}\right]d\theta \tag{39}$$

where ϵ_{mb} is the membrane strain during buckling given by

$$\epsilon_{mb} = \tilde{w}_b' - \tilde{v}_b + \tilde{v}'\tilde{v}_b' \tag{40}$$

The functions $\tilde{w}_b$ and $\tilde{v}_b$ which make the functional $(1/2)\delta^2 V^*$ stationary satisfy the Euler–Lagrange equations of variational calculus, which leads to

$$\epsilon'_{mb} = 0 \tag{41}$$

in the axial direction so that the membrane strain ϵ_{mb} during buckling is a constant, and to the buckling differential equilibrium equation

$$\frac{\tilde{v}_b^{iv}}{\mu^2} + \tilde{v}_b'' = \frac{R^2 \epsilon_{mb}}{r_x^2 \mu^2}(1 + \tilde{v}'') \tag{42}$$

in the radial direction.

4.2. Buckling of pin-ended shallow arches

For anti-symmetric bifurcation buckling, the dimensionless buckling displacement $\tilde{v}_b$ is anti-symmetric while the dimensionless pre-buckling displacement $\tilde{v}$ is symmetric, so that the terms $\tilde{v}_b$ and $\tilde{v}'\tilde{v}'_b$ are anti-symmetric and their integrals within the interval $[-\Theta, \Theta]$ vanish. In addition, the boundary conditions require that $\tilde{w}_b = 0$ at $\theta = \pm\Theta$, so that the average strain ϵ_{mb} during buckling is obtained as

$$\epsilon_{mb} = \frac{1}{2\Theta}\int_{-\Theta}^{\Theta} \epsilon_{mb}\, d\theta = \frac{1}{2\Theta}\int_{-\Theta}^{\Theta}\left(\tilde{w}'_b - \frac{\tilde{v}_b}{R} + \tilde{v}'\tilde{v}'_b\right) d\theta = 0 \tag{43}$$

Substituting $\epsilon_{mb} = 0$ into Eq. (42) leads to the linear homogeneous differential equation for anti-symmetric buckling of shallow arches given by

$$\frac{\tilde{v}_b^{iv}}{\mu^2} + \tilde{v}_b'' = 0 \tag{44}$$

The solution of Eq. (44) that satisfies the boundary conditions $\tilde{v}_b = 0$ at $\theta = \pm\Theta$ is

$$\tilde{v}_b = C\left[\sin(\mu\theta) - \frac{\theta \sin(\mu\Theta)}{\Theta}\right] \tag{45}$$

where C is an amplitude parameter.

For pin-ended arches, using the boundary conditions $\tilde{v}''_b = 0$ at $\theta = \pm\Theta$, Eq. (45) leads to

$$\sin(\mu\Theta) = 0 \tag{46}$$

whose fundamental solution is

$$\mu\Theta = \pi \tag{47}$$

so that from Eq. (23) the corresponding actual axial compression $\overline{N}$ in a pin-ended arch is

$$\overline{N} = \frac{\pi^2 E I_x}{(R\Theta)^2} = \frac{\pi^2 E I_x}{(S/2)^2} = N_P \tag{48}$$

Substituting Eq. (47) into the non-linear equilibrium condition (29) leads to

$$(2\pi^2 + 15)\bar{q}^2 + (4\pi^2 + 12)\bar{q} + \frac{12\pi^4}{\lambda_s^2} = 0 \tag{49}$$

and solving the quadratic equation (49) for $\bar{q}$ leads to the anti-symmetric buckling load of a pin-ended shallow arch given by

$$N_{sb} = q_{sb}R = \frac{9 \pm \sqrt{(2\pi^2+6)^2 - 12(2\pi^2+15)\pi^4/\lambda_s^2}}{2\pi^2+15} N_P \tag{50}$$

which can be simplified to

$$N_{sb} = q_{sb}R \approx \left(0.26 \pm 0.74\sqrt{1 - 0.63\frac{\pi^4}{\lambda_s^2}}\right) N_P \tag{51}$$

When $\lambda_s \geqslant \sqrt{0.63}\pi^2 \approx 7.83$, a real anti-symmetric buckling solution in Eq. (51) exists, so that anti-symmetric buckling of the pin-ended arch may occur.

For the symmetric snap-through buckling of a pin-ended arch, the dimensionless buckling displacement v_b is symmetric. Substituting Eq. (25) into Eq. (42) leads to the buckling equilibrium equation

$$\frac{\tilde{v}_b^{iv}}{\mu^2} + \tilde{v}_b'' = \frac{R^2\epsilon_{mb}}{r_x^2\mu^2}\left\{1 + \bar{q}\left[1 - \frac{\cos(\mu\theta)}{\cos(\mu\Theta)}\right]\right\} \tag{52}$$

The solution of Eq. (52), which satisfies the boundary conditions $\tilde{v}_b = \tilde{v}_b'' = 0$ at $\theta = \Theta$, is

$$\tilde{v}_b = \frac{R^2}{r_x^2}\frac{\epsilon_{mb}}{\mu^4}\left\{\frac{1+\bar{q}}{2}[(\mu\theta)^2 - (\mu\Theta)^2] + (1+2\bar{q})\frac{\cos(\mu\theta) - \cos(\mu\Theta)}{\cos(\mu\Theta)} + \frac{\bar{q}}{2}\left[\frac{(\mu\theta)\sin(\mu\theta)}{\cos(\mu\Theta)} - \frac{(\mu\Theta)\cos(\mu\theta)\sin(\mu\Theta)}{\cos^2(\mu\Theta)}\right]\right\} \tag{53}$$

The average buckling membrane strain of Eq. (40) over the arch is equal to the constant buckling membrane strain ϵ_{mb}, which leads to an equation for the relationship between the dimensionless load $\bar{q}$ and angle $\mu\Theta$ during symmetric snap-through buckling given by

$$A_3\bar{q}^2 + B_3\bar{q} + C_3 = 0 \tag{54}$$

where

$$A_3 = 2A_1 + D_3 \tag{55}$$

$$B_3 = 4A_1 \tag{56}$$

and

$$C_3 = B_1 - C_1 \tag{57}$$

and A_1, B_1 and C_1 are given by Eqs. (30)–(32) and D_3 is given by

$$D_3 = \frac{7\tan^2(\mu\Theta)}{8(\mu\Theta)^2} + \frac{15}{8(\mu\Theta)^2} - \frac{15\tan(\mu\Theta)}{8(\mu\Theta)^3} - \frac{\tan(\mu\Theta)}{4\mu\Theta} - \frac{\tan^3(\mu\Theta)}{4\mu\Theta} \tag{58}$$

For a given value of μ, a solution of the symmetric snap-through buckling load $N_{ss} = q_{ss}R$ and the corresponding value of λ_s can be obtained by solving Eqs. (29) and (54) simultaneously. However, the value of λ_s rather than the value of μ is usually known for a shallow arch. In this case, an iterative process needs to be used to obtain a solution of $N_{ss} = q_{ss}R$ by solving Eqs. (29) and (54) simultaneously.

The value of the modified slenderness λ_s that defines a switch between the buckling modes can be found when $N_{ss} = N_{sb}$ at $\mu\Theta = \pi$, which leads to $\lambda_s \approx 9.38$. When $\lambda_s > 9.38$, a pin-ended arch may buckle in an anti-symmetric mode, but when $7.83 \leqslant \lambda_s \leqslant 9.38$, both symmetric and anti-symmetric buckling may occur. It will be shown next that symmetric buckling occurs first and that anti-symmetric buckling occurs on the

descending branch of load–displacement curve. When the modified slenderness $\lambda_s < 7.83$, the pin-ended arch may buckle only in a symmetric mode.

Because the iterative solution process for the symmetric buckling load of an arch is complicated, an approximation for the symmetric buckling load of a pin-ended arch whose modified slenderness $\lambda_s \leqslant 9.38$ is proposed as

$$N_{ss} = q_{ss}R \approx (0.15 + 0.006\lambda_s^2)N_P \tag{59}$$

The lowest value of the symmetric buckling load $N_{ss} = q_{ss}R$ for a pin-ended arch can be obtained from Eq. (29) as (Pi and Bradford, 2000)

$$\lim_{\mu\Theta\to\pi/2} \bar{q} = \lim_{\mu\Theta\to\pi/2} \frac{qR - \overline{N}}{\overline{N}} = 0 \tag{60}$$

which leads to

$$N_{ss} = q_{ss}R = \lim_{\mu\Theta\to\pi/2} \overline{N} = \lim_{\mu\Theta\to\pi/2} \frac{\mu^2 EI_x}{R^2} = \frac{\pi^2 EI_x}{S^2} \tag{61}$$

From Eq. (25), the dimensionless central radial displacement $\tilde{v}_c$ of a pin-ended arch ($\theta = 0$) is

$$\tilde{v}_c = \frac{\bar{q}}{\mu^2}\left[\frac{1}{\cos(\mu\Theta)} - 1 - \frac{(\mu\Theta)^2}{2}\right] \tag{62}$$

Hence, the corresponding dimensionless central radial displacement $\tilde{v}_c$ at $N_{ss} = \pi^2 EI_x/S^2$ can be obtained from Eq. (62) as (Pi and Bradford, 2000)

$$\lim_{\mu\Theta\to\pi/2} \tilde{v}_c = \frac{4S^2}{\pi^3 R^2}\left(1 \pm \sqrt{1 - \frac{\pi^6}{64\lambda_s^2}}\right) \tag{63}$$

The value of the central radial displacement v_c is real when $1 - (\pi^6/64\lambda_s^2) \geqslant 0$, that is when $\lambda_s \geqslant \pi^3/8$ ($\approx$3.88). When $\lambda_s < 3.88$, buckling of a pin-ended arch does not occur.

The solution (51) for the anti-symmetric buckling and the approximation (59) for the symmetric buckling of a pin-ended arch are compared with finite element predictions in Figs. 3 and 4. The solution for

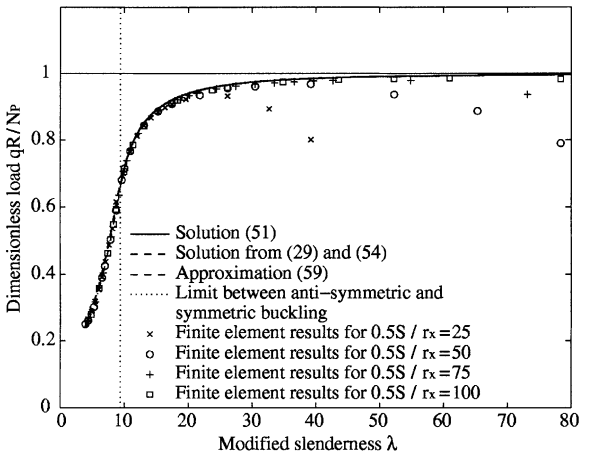

Fig. 3. Buckling load of pin-ended arches against slenderness.

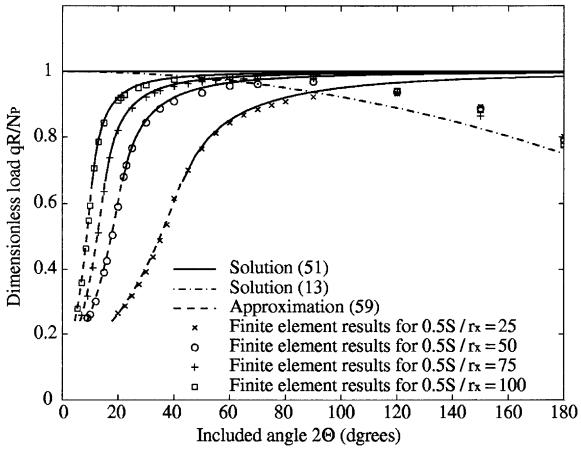

Fig. 4. Buckling load of pin-ended arches against included angle.

symmetric buckling obtained by simultaneously solving Eqs. (29) and (54) is also shown in Fig. 3, while the classical buckling load (13) for pin-ended arches is also shown in Fig. 4. Fig. 3 shows the variation of the dimensionless buckling load qR/N_P with the modified slenderness λ_s, where q is the buckling load and N_P is the classical anti-symmetric buckling load of a pin-ended arch given by Eq. (10). Fig. 4 shows the variation of the dimensionless buckling load qR/N_P with the included angle 2Θ. The finite element package ABAQUS (1998) and the finite element program developed by Pi and Trahair (1998) were used in the numerical analysis, and the results of ABAQUS are identical to those of Pi and Trahair. In the finite element analysis, an I-section, a rectangular hollow section and a rectangular solid section were used. The dimensions of the I-section are: the overall depth $D = 0.2613$ m, the flange width $B = 0.151$ m, the flange thickness $t_f = 0.0123$ m, and the web thickness $t_w = 0.0077$ m. The dimensions of the rectangular hollow section are: the overall height $D = 0.4$ m and the width $B = 0.25$ m and the wall-thickness $t = 0.003$ m. The dimensions of the rectangular solid section are: the height $D = 0.005$ m and the width $B = 0.010$ m. The Young' modulus of elasticity is assumed to be equal to $E = 200{,}000$ MPa for the three sections.

It can be observed from Figs. 3 and 4 that when the included angle $2\Theta \leqslant 90°$, the approximation (59) is almost identical to the solution from Eqs. (29) and (54) for the symmetric buckling of pin-ended arches with the modified slenderness $\lambda_s \leqslant 9.38$. Both of these agree extremely well with the finite element predictions. The solution (51) for anti-symmetric buckling almost coincides with the finite element results for pin-ended arches with the modified slenderness $\lambda_s \geqslant 9.38$ and the included angle $2\Theta \leqslant 90°$. The classical buckling loads of either Eqs. (10) or (13) are much higher than the finite element predictions for pin-ended arches with the included angle $2\Theta \leqslant 90°$.

When the included angle $2\Theta \geqslant 90°$, the solution (51) approaches the classical buckling load (10) with the increase of the modified slenderness and the included angle 2Θ, and tends to be higher than the finite element predictions. The classical buckling load (13) provides a good lower bound prediction for the anti-symmetric buckling of pin-ended arches. The included angle $2\Theta = 90°$ can be used as a criterion for distinguishing between shallow and non-shallow pin-ended arches based on the in-plane instability under radial loading.

4.3. Buckling of fixed shallow arches

For anti-symmetric buckling of fixed shallow arches, using the boundary condition $\tilde{v}_b = \tilde{v}'_b = 0$ at $\theta = \pm\Theta$ in Eq. (45) produces

$$\tan(\mu\Theta) = \mu\Theta \tag{64}$$

The lowest solution of Eq. (64) is

$$\mu\Theta \approx 1.4303\pi \tag{65}$$

so that from Eq. (23) the corresponding actual axial compression $\overline{N}$ in a fixed arch at anti-symmetric buckling is

$$\overline{N} \approx \frac{(1.4303\pi)^2 EI_x}{(S/2)^2} = N_{\mathrm{FB}} \tag{66}$$

Substituting Eqs. (64) and (65) into Eq. (35) leads to

$$5\bar{q}^2 + 4\bar{q} + \frac{12(1.4303\pi)^2}{\lambda_s^2} = 0 \tag{67}$$

and solving Eq. (67) for $\bar{q}$ leads to the anti-symmetric buckling load of fixed shallow arches given by

$$N_{\mathrm{sb}} = q_{\mathrm{sb}} R = \frac{3 \pm 2\sqrt{1 - 15(1.4303\pi)^2/\lambda_s^2}}{5} N_{\mathrm{FB}} \tag{68}$$

which can be simplified to

$$N_{\mathrm{sb}} \approx \left(0.6 \pm 0.4\sqrt{1 - 30.686\frac{\pi^2}{\lambda_s^2}}\right) N_{\mathrm{FB}} \tag{69}$$

When $\lambda_s \geqslant \sqrt{30.686}\pi \approx 17.40$, a real anti-symmetric buckling solution (69) exists, so that anti-symmetric buckling of the fixed arch may occur. The solution (69) can be reduced to that obtained by Schreyer and Masur (1966) for fixed arches with a rectangular solid section.

For symmetric snap-through buckling of fixed arches, substituting Eq. (34) into Eq. (42) leads to the buckling equilibrium equation

$$\frac{\tilde{v}_{\mathrm{b}}^{iv}}{\mu^2} + \tilde{v}_{\mathrm{b}}'' = \frac{R^2 \epsilon_{\mathrm{mb}}}{r_x^2 \mu^2}\left\{1 + \bar{q}\left[1 - \frac{(\mu\Theta)\cos(\mu\theta)}{\sin(\mu\Theta)}\right]\right\} \tag{70}$$

The solution of Eq. (70), which satisfies the boundary conditions $\tilde{v}_{\mathrm{b}} = \tilde{v}_{\mathrm{b}}' = 0$ at $\theta = \Theta$, is

$$\tilde{v}_{\mathrm{b}} = \frac{R^2}{r_x^2}\frac{\epsilon_{\mathrm{mb}}}{\mu^4}\left\{\frac{1+\bar{q}}{2}[(\mu\theta)^2 - (\mu\Theta)^2] + \left(1 + \frac{3\bar{q}}{2}\right)\left[\frac{(\mu\Theta)(\cos(\mu\theta) - \cos(\mu\Theta))}{(\sin\mu\Theta)}\right] + \frac{\bar{q}}{2}\left[\frac{(\mu\theta)(\mu\Theta)\sin(\mu\theta)}{\sin(\mu\Theta)} + \frac{(\mu\Theta)^2(\cos(\mu\theta)\cos(\mu\Theta) - 1)}{\sin^2(\mu\Theta)}\right]\right\} \tag{71}$$

The average buckling membrane strain of Eq. (40) over the arch is equal to the constant buckling membrane strain ϵ_{mb}, which leads to an equation for the relationship between the dimensionless load $\bar{q}$ and angle $\mu\Theta$ during symmetric snap-through buckling given by

$$A_4\bar{q}^2 + B_4\bar{q} + C_4 = 0 \tag{72}$$

where

$$A_4 = 2A_2 + D_4 \tag{73}$$

$$B_4 = 4A_2 \tag{74}$$

and

$$C_4 = B_2 - C_2 \tag{75}$$

and A_2, B_2 and C_2 are given by Eqs. (36)–(38) and D_4 is given by

$$D_4 = \frac{1}{2} + \frac{(\mu\Theta)\cot(\mu\Theta)}{4} + \frac{1}{(\mu\Theta)^2}\left[\frac{3}{4}(\mu\Theta)^2\cot^2(\mu\Theta) + \frac{1}{4}(\mu\Theta)^3\cot^3(\mu\Theta) - 1\right] \tag{76}$$

For a value of μ, a solution for the symmetric snap-through buckling load $N_{ss} = q_{ss}R$ and the corresponding value of λ_s can be obtained by solving Eqs. (35) and (72) simultaneously. However, again the value of λ_s rather than the value of μ is usually known for a shallow arch. In this case, an iterative process needs to be used to obtain a solution of $N_{ss} = q_{ss}R$ by solving Eqs. (35) and (72) simultaneously.

The value of the modified slenderness λ_s for distinguishing between the buckling modes can be found when $N_{ss} = N_{sb}$ at $\mu\Theta = 1.4303\pi$. This leads to $\lambda_s \approx 18.60$, but when $\lambda_s > 18.60$, the fixed arch may buckle in an anti-symmetric mode. When $17.40 \leqslant \lambda_s \leqslant 18.60$, both symmetric and anti-symmetric buckling may occur. It will be shown next that symmetric buckling occurs first and that anti-symmetric buckling occurs on the descending branch of the load–displacement curve. When the modified slenderness $\lambda_s < 17.40$, the fixed arch may buckle only in a symmetric mode.

Alternatively, the symmetric buckling of pin-ended and fixed arches can be obtained by finding the maximum value of q by differentiating Eqs. (29) or (35) for pin-ended arches or fixed arches respectively as

$$\frac{d\bar{q}}{d(\mu\Theta)} = 0 \tag{77}$$

However, implementing this process becomes very complicated and is not pursued further herein.

Because the solution processes for a symmetric buckling mode are complicated, an approximation for the symmetric buckling load of fixed arches with the modified slenderness $\lambda_s \leqslant 18.60$ is proposed as

$$N_{ss} = q_{ss}R \approx (0.36 + 0.0011\lambda_s^2)N_P \tag{78}$$

The lowest value of the symmetric buckling load $N_{ss} = q_{ss}R$ for a fixed arch can be obtained from Eq. (35) as (Pi and Bradford, 2000)

$$\lim_{\mu\Theta\to\pi}\bar{q} = \lim_{\mu\Theta\to\pi}\frac{qR - \overline{N}}{\overline{N}} = 0 \tag{79}$$

which leads to

$$N_{ss} = q_{ss}R = \lim_{\mu\Theta\to\pi}\overline{N} = \lim_{\mu\Theta\to\pi}\frac{\mu^2 EI_x}{R^2} = \frac{\pi^2 EI_x}{(S/2)^2} \tag{80}$$

From Eq. (34), the dimensionless central radial displacement $\tilde{v}_c$ of the fixed arch ($\theta = 0$) is

$$\tilde{v}_c = \frac{\bar{q}}{\mu^2}\left\{\frac{(\mu\Theta)[1 - \cos(\mu\Theta)]}{\sin(\mu\Theta)} - \frac{(\mu\Theta)^2}{2}\right\} \tag{81}$$

Thus, the corresponding dimensionless central radial displacement $\tilde{v}_c$ at $N_{ss} = \pi^2 EI_x/(S/2)^2$ can be obtained from Eq. (81) as (Pi and Bradford, 2000)

$$\lim_{\mu\Theta\to\pi}\tilde{v}_c = \frac{S^2}{\pi^2 R^2}\left(1 \pm \sqrt{1 - \frac{\pi^4}{\lambda_s^2}}\right) \tag{82}$$

The value of the central radial displacement v_c is real when $1 - (\pi^4/\lambda_s^2) \geqslant 0$, that is when $\lambda_s \geqslant \pi^2(\approx 9.87)$. When the modified slenderness $\lambda_s \leqslant 9.87$, buckling of a fixed shallow arch does not occur.

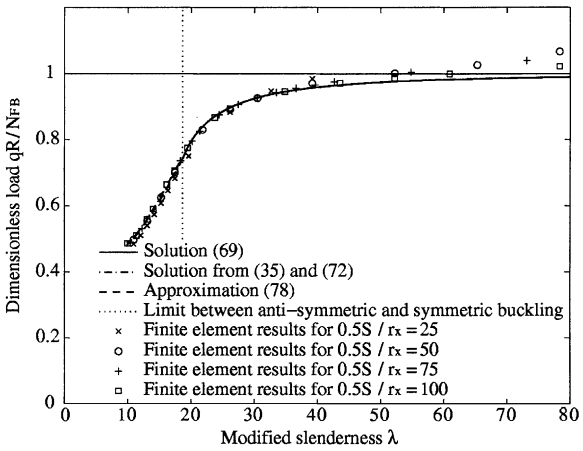

Fig. 5. Buckling load of fixed arches against slenderness.

The solutions (69) for the anti-symmetric buckling and the approximation (78) for the symmetric buckling of fixed arches are compared with finite element results in Figs. 5 and 6. The solutions for symmetric buckling obtained by simultaneously solving Eqs. (35) and (72) are also shown in Fig. 5, while the classical buckling load (12) for fixed arches is also shown in Fig. 6. In the finite element analysis, the cross-sections and material properties are the same as those used for the pin-ended arches.

It can be observed that the approximation (78) is almost identical to the solution obtained from Eqs. (35) and (72) for the symmetric buckling of fixed arches with the modified slenderness $\lambda_s \leqslant 18.60$. Both of these agree with the finite element results very well. The solution (69) for anti-symmetric buckling almost coincides with the finite element results for fixed arches with the included angle $2\Theta \leqslant 90°$. The classical buckling loads of both Eqs. (12) and (14) are much higher than the finite element predictions for fixed arches with the included angle $2\Theta < 90°$.

The classical buckling load (11) provides a good prediction for the anti-symmetric buckling of fixed arches with $2\Theta \geqslant 90°$. The included angle $2\Theta = 90°$ can be used as a criterion for distinguishing between

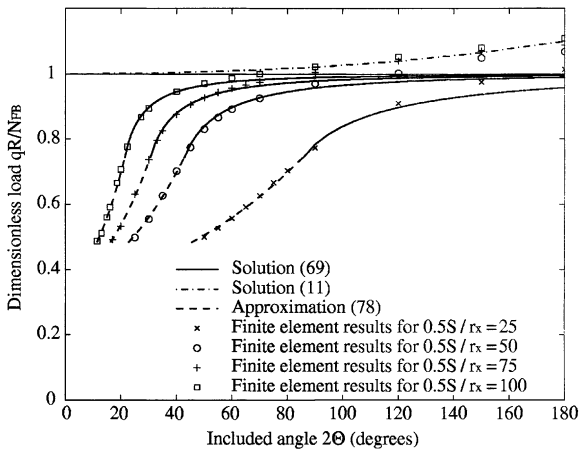

Fig. 6. Buckling load of fixed arches against included angle.

shallow and non-shallow arches. The solution (69) approaches the second mode classical buckling load (12) of the corresponding fixed column with the increase of the modified slenderness λ_s and included angle 2Θ, and tends to be slightly lower than the finite element results. Hence, the solution (69) can be used to predict the buckling load accurately for fixed shallow arches and approximately for fixed non-shallow arches when the modified slenderness $\lambda_s \geqslant 18.60$.

4.4. Structural behaviour of arches

Typical variations of the dimensionless central vertical displacement v_c/f with the dimensionless axial load qR/N_P for pin-ended shallow arches are shown in Fig. 7, with Fig. 8 showing the counterparts for fixed shallow arches, where f is the arch rise. Four types of buckling and post-buckling behaviour can be observed in these figures. For the first type, there is no buckling as shown in Figs. 7(a) and 8(a). Pin-ended arches with a modified slenderness $\lambda_s \leqslant 3.88$ and fixed arches with $\lambda_s \leqslant 9.87$ belong to this type. For the second type, the arches buckle in a symmetric mode without bifurcation as shown in Figs. 7(b) and 8(b). Pin-ended arches with a modified slenderness $3.88 \leqslant \lambda_s \leqslant 7.83$ and fixed arches with $9.87 \leqslant \lambda_s \leqslant 17.40$ are in this category. For the third type, the arches buckle in the symmetric snap-through mode first and then bifurcate anti-symmetrically on the descending branch of the load–deflection curve under deflection control as shown in Figs. 7(c) and 8(c). Pin-ended arches with a modified slenderness $7.83 \leqslant \lambda_s \leqslant 9.38$ and fixed arches with $17.40 \leqslant \lambda_s \leqslant 18.60$ display this behaviour. For the fourth type, the arches undergo anti-symmetric bifurcation buckling, and the load carrying capacity of the arches decrease rapidly after this as shown in Figs. 7(d) and 8(d). Pin-ended shallow arches with a modified slenderness $\lambda_s \geqslant 9.38$ and fixed shallow arches with $\lambda_s \geqslant 18.60$ belong to this type. It can be seen from Figs. 7 and 8 that the deflections are substantial when buckling occurs so that classical buckling theory, which does not consider the effects of pre-buckling deformations on buckling, cannot be used to predict the buckling load of shallow arches and moreover is unconservative.

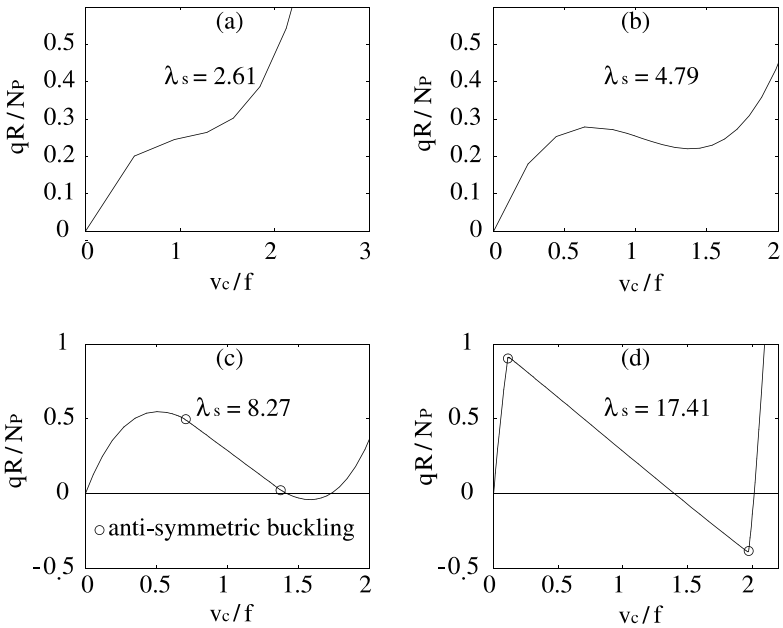

Fig. 7. Buckling and post-buckling behaviour of pin-ended arches.

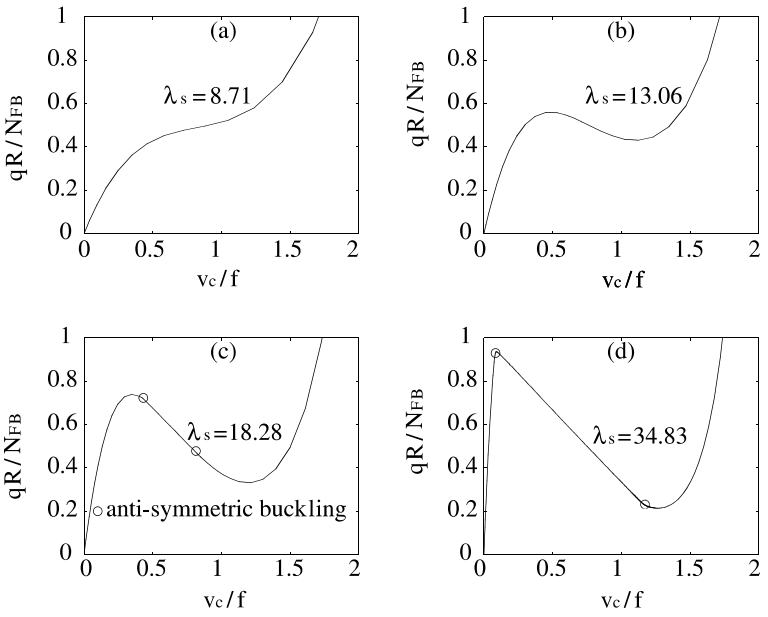

Fig. 8. Buckling and post-buckling behaviour of fixed arches.

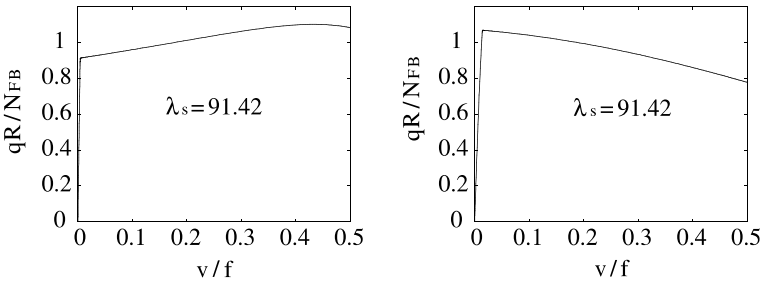

Fig. 9. Buckling and post-buckling behaviour of non-shallow arches.

The buckling and post-buckling behaviour of non-shallow arches is illustrated in Fig. 9. The buckling mode is characterised by anti-symmetric bifurcation, but the post-buckling loads of pin-ended arches increase slightly while the post-buckling loads of fixed arches decrease slightly. The deflections are very small when buckling occurs. This indicates that the effects of pre-buckling deformations on the buckling of non-shallow arches can be ignored and classical buckling theory can be used to predict their buckling load.

5. Concluding remarks

This paper has studied the in-plane stability of both pin-ended and fixed uniform circular arches with an arbitrary cross-section subjected to a radial load uniformly distributed around the arch axis. It has been found that classical buckling theory overestimates both the symmetric snap-through buckling and the anti-symmetric bifurcation buckling load of shallow arches. Non-linear analysis based on an energy method

developed in this paper provides accurate solutions for the symmetric and anti-symmetric buckling of both pin-ended and fixed shallow arches. The solutions include the non-linear effect of the pre-buckling deformations due to the bending action. Approximate solutions have been proposed for the symmetric buckling load of pin-ended and fixed shallow arches. Comparisons with finite element predictions have shown that the closed form solutions (51) and (69) for the anti-symmetric buckling load of pin-ended and fixed shallow arches and the approximations (59) and (78) for the symmetric buckling load of pin-ended and fixed shallow arches are accurate.

The criteria for the classification of different types of fundamental buckling behaviour have been established. The included angle $2\Theta = 90°$ can be used as a criterion for distinguishing between shallow and non-shallow arches. For pin-ended arches with the included angle $2\Theta \leqslant 90°$, the solution (51) can be used to predict the anti-symmetric bifurcation buckling load of shallow arches whose modified slenderness $\lambda_s \geqslant 9.38$, while the approximation (59) can be used to predict the symmetric buckling load of arches with $3.88 \leqslant \lambda_s \leqslant 9.38$. For fixed arches with the included angle $2\Theta \leqslant 90°$, the solution (69) can be used to predict the anti-symmetric bifurcation buckling load when the modified slenderness $\lambda_s \geqslant 18.60$ while the approximation (78) can be used to predict the symmetric buckling load when $9.878 \leqslant \lambda_s < 18.60$. Buckling does not occur for pin-ended arches with the modified slenderness $\lambda_s \leqslant 3.88$ or for fixed arches with the modified slenderness $\lambda_s \leqslant 9.87$. When the included angle $2\Theta \geqslant 90°$, the anti-symmetric bifurcation buckling load for pin-ended non-shallow arches can be predicted by the classical solution (13), while the anti-symmetric bifurcation buckling load for fixed non-shallow arches can be predicted by the classical solution (11).

Acknowledgements

This work has been supported by a research grant made available by the Australian Research Council under the ARC Large Research Grant Scheme.

Appendix A. Limit value of buckling load

The lowest symmetric buckling load can be obtained as follows. From Eq. (29)

$$\bar{q} = \frac{-B_1 \pm \sqrt{B_1^2 - 4A_1C_1}}{2A_1} \tag{A.1}$$

so that the dimensionless load $\bar{q}$ of pin-ended arches at $\mu\Theta = \pi/2$ can be obtained as

$$\lim_{\mu\Theta\to\pi/2} \bar{q} = \lim_{\mu\Theta\to\pi/2} \frac{(-B_1 \pm \sqrt{B_1^2 - 4A_1C_1})(\pi/2 - \mu\Theta)^2}{2A_1(\pi/2 - \mu\Theta)^2} \tag{A.2}$$

Because

$$\begin{aligned}\lim_{\mu\Theta\to\pi/2} A_1(\pi/2 - \mu\Theta)^2 &= \lim_{\mu\Theta\to\pi/2} \left\{ \frac{1}{4(\mu\Theta)^2}\left[5 - 5\frac{\tan(\mu\Theta)}{\mu\Theta} + \tan^2(\mu\Theta)\right] + \frac{1}{6}\right\}\left(\frac{\pi}{2} - \mu\Theta\right)^2 \\ &= \lim_{\mu\Theta\to\pi/2} \left\{ \frac{1}{4(\mu\Theta)^2}\left[5\left(\frac{\pi}{2} - \mu\Theta\right)^2 - 5\frac{\cot(\pi/2 - \mu\Theta)}{\mu\Theta}\left(\frac{\pi}{2} - \mu\Theta\right)^2 \right.\right. \\ &\quad \left.\left. + \cot^2\left(\frac{\pi}{2} - \mu\Theta\right)\left(\frac{\pi}{2} - \mu\Theta\right)^2\right] + \frac{1}{6}\left(\frac{\pi}{2} - \mu\Theta\right)^2\right\} = \frac{1}{\pi^2}\end{aligned} \tag{A.3}$$

and

$$\lim_{\mu\Theta\to\pi/2} B_1(\pi/2-\mu\Theta) = \lim_{\mu\Theta\to\pi/2}\left\{\frac{1}{(\mu\Theta)^2}\left[1-\frac{\tan(\mu\Theta)}{\mu\Theta}\right]+\frac{1}{3}\right\}\left(\frac{\pi}{2}-\mu\Theta\right)$$
$$= \lim_{\mu\Theta\to\pi/2}\left\{\frac{1}{(\mu\Theta)^2}\left[\left(\frac{\pi}{2}-\mu\Theta\right)-\frac{\cot(\pi/2-\mu\Theta)}{\mu\Theta}\left(\frac{\pi}{2}-\mu\Theta\right)\right]+\frac{1}{3}\left(\frac{\pi}{2}-\mu\Theta\right)\right\}$$
$$= -\frac{8}{\pi^3} \tag{A.4}$$

the dimensionless load $\bar{q}$ of pin-ended shallow arches at $\mu\Theta=\pi/2$ is equal to zero

$$\lim_{\mu\Theta\to\pi/2}\bar{q}=0 \tag{A.5}$$

Because

$$\lim_{\mu\Theta\to\pi/2}\frac{\bar{q}}{(\pi/2-\mu\Theta)} = \lim_{\mu\Theta\to\pi/2}\frac{(-B_1\pm\sqrt{B_1^2-4A_1C_1})(\pi/2-\mu\Theta)}{2A_1(\pi/2-\mu\Theta)^2} = \frac{4}{\pi}\left(1\pm\sqrt{1-\frac{\pi^6}{64\lambda_s^2}}\right) \tag{A.6}$$

the corresponding dimensionless central vertical displacement $\tilde{v}_c$ of a pin-ended arch at $\mu S/2=\pi/2$ can then be obtained from Eq. (62) as

$$\lim_{\mu\Theta\to\pi/2}\tilde{v}_c = \lim_{\mu\Theta\to\pi/2}\frac{1}{\mu^2}\frac{\bar{q}}{(\pi/2-\mu\Theta)}\left[\frac{(\pi/2-\mu\Theta)}{\sin(\pi/2-\mu\Theta)}-\left(\frac{\pi}{2}-\mu\Theta\right)\left(1+\frac{(\mu\Theta)^2}{2}\right)\right]$$
$$= \frac{4S^2}{\pi^3R^2}\left(1\pm\sqrt{1-\frac{\pi^6}{64\lambda_s^2}}\right) \tag{A.7}$$

The value of $\tilde{v}_c$ is real when $1-(\pi^6/64\lambda_s^2)\geqslant 0$, so that $\lambda_s\geqslant\pi^3/8=3.88$. When $\lambda_s<3.88$, there is no buckling for pin-ended arches.

The lowest symmetric buckling load can be obtained as follows. From Eq. (35)

$$\bar{q}=\frac{-B_2\pm\sqrt{B_2^2-4A_2C_2}}{2A_2} \tag{A.8}$$

the dimensionless load $\bar{q}$ of fixed arches at $\mu\Theta=\pi$ can be obtained from Eq. (81) as

$$\lim_{\mu\Theta\to\pi}\bar{q} = \lim_{\mu\Theta\to\pi}\frac{(-B_2\pm\sqrt{B_2^2-4A_2C_2})(\pi-\mu\Theta)^2}{2A_2(\pi-\mu\Theta)^2} \tag{A.9}$$

Because

$$\lim_{\mu\Theta\to\pi}A_2(\pi-\mu\Theta)^2 = \lim_{\mu\Theta\to\pi}\left\{\frac{5}{12}+\frac{1}{4(\mu\Theta)^2}[3(\mu\Theta)\cot(\mu\Theta)+(\mu\Theta)^2\cot^2(\mu\Theta)-4]\right\}(\pi-\mu\Theta)^2$$
$$= \lim_{\mu\Theta\to\pi}\left\{\frac{5}{12}(\pi-\mu\Theta)^2+\frac{1}{4(\mu\Theta)^2}[-3(\mu\Theta)\cot(\pi-\mu\Theta)(\pi-\mu\Theta)^2\right.$$
$$\left.+(\mu\Theta)^2\cot^2(\pi-\mu\Theta)(\pi-\mu\Theta)^2-4(\pi-\mu\Theta)^2]\right\}$$
$$= \frac{1}{4} \tag{A.10}$$

and

$$\lim_{\mu\Theta\to\pi} B_2(\pi-\mu\Theta) = \lim_{\mu\Theta\to\pi}\left\{\frac{1}{3}+\frac{1}{(\mu\Theta)^2}[(\mu\Theta)\cot(\mu\Theta)-1]\right\}(\pi-\mu\Theta)$$
$$= \lim_{\mu\Theta\to\pi}\left\{\frac{1}{3}(\pi-\mu\Theta)+\frac{1}{(\mu\Theta)^2}[-(\mu\Theta)\cot(\pi-\mu\Theta)(\pi-\mu\Theta)-(\pi-\mu\Theta)]\right\}$$
$$= -\frac{1}{\pi} \tag{A.11}$$

the dimensionless load $\bar{q}$ of a fixed arch at $\mu\Theta=\pi$ is equal to zero

$$\lim_{\mu\Theta\to\pi}\bar{q}=0 \tag{A.12}$$

Because

$$\lim_{\mu\Theta\to\pi}\frac{\bar{q}}{\pi-\mu\Theta} = \lim_{\mu\Theta\to\pi}\frac{(-B_2\pm\sqrt{B_2^2-4A_2C_2})(\pi-\mu\Theta)}{2A_2(\pi-\mu\Theta)^2} = \frac{2}{\pi}\left(1\pm\sqrt{1-\frac{\pi^4}{\lambda_s^2}}\right) \tag{A.13}$$

the dimensionless central vertical displacement $\tilde{v}_c$ at $\mu\Theta=\pi$ is obtained as

$$\lim_{\mu\Theta\to\pi}\tilde{v}_c = \lim_{\mu\Theta\to\pi}\frac{1}{\mu^2}\frac{\bar{q}}{(\pi-\mu\Theta)}\left\{\frac{\mu\Theta[1+\cos(\pi-\mu\Theta)](\pi-\mu\Theta)}{\sin(\pi-\mu\Theta)}-(\pi-\mu S/2)\frac{(\mu\Theta)^2}{2}\right\}$$
$$= \frac{S^2}{\pi^2R^2}\left(1\pm\sqrt{1-\frac{\pi^4}{\lambda_s^2}}\right) \tag{A.14}$$

The value of $\tilde{v}_c$ is real when $1-(\pi^4/\lambda_s^2)\geqslant 0$, so that $\lambda_s\geqslant\pi^2=9.87$. When $\lambda_s<9.87$, there is no buckling for fixed shallow arches.

References

ABAQUS Standard User's Manual version 5.8, 1998. Hibbit, Karlsson and Sorensen Inc., Abaqus, Pawtucket, Rhode Island.

AS4100 Steel structures, 1998. Standards Australia, Sydney, Australia.

BS5950 Structural use of steelwork in building. Part I: code of practice for design in simple and continuous construction, 1998. British Standards Institution, London, UK.

Calhoun, P.R., DaDeppo, D.A., 1983. Nonlinear finite element analysis of clamped arches. Journal of Structural Engineering ASCE 109 (3), 599–612.

Dickie, J.F., Broughton, P., 1971. Stability criteria for shallow arches. Journal of the Engineering Mechanics Division ASCE 97 (EM3), 951–965.

Elias, Z.M., Chen, K.L., 1988. Nonlinear shallow curved beam finite element. Journal of Engineering Mechanics ASCE 114 (6), 1076–1087.

Gjelsvik, A., Bodner, S.R., 1962. Energy criterion and snap-through buckling of arches. Journal of the Engineering Mechanics Division ASCE 88 (EM5), 87–134.

Galambos, T.V. (Ed.), 1988. Guide to Stability Design Criteria for Metal Structures, fourth ed. Wiley, New York.

Handbook of structural stability, 1971. Edited by Column Research Committee of Japan. Corona publishing Company, Tokyo.

Hodges, D.H., 1999. Non-linear in-plane deformation and buckling of rings and high arches. International Journal of Non-Linear Mechanics 34 (4), 723–737.

Johnston, B.G. (Ed.), 1976. Guide to Stability Design Criteria for Metal Structures, third ed. Wiley, New York.

Kang, Y.J., Yoo, C.H., 1994. Thin-walled curved beams. II: analytical solutions for buckling of arches. Journal of Engineering Mechanics ASCE 120 (10), 2102–2125.

Load and resistance factor design specification for structural steel building, 1993. American Institute of Steel Construction, Chicago, Ill, USA.

Noor, A.K., Peters, J.M., 1981. Mixed model and reduced/selective integration displacement model for nonlinear analysis of curved beams. International Journal for Numerical Methods in Engineering 17 (4), 615–631.

Papangelis, J.P., Trahair, N.S., 1987. Flexural-torsional buckling of arches. Journal of Structural Engineering ASCE 113 (4), 889–906.

Pi, Y.-L., Bradford, M.A., 2000. In-plane stability of arches. UNICIV Report no. xx, School of Civil and Environmental Engineering. The University of New South Wales, Sydney.

Pi, Y.-L., Trahair, N.S., 1998. Non-linear buckling and postbuckling of elastic arches. Engineering Structures 20 (7), 571–579.

Pi, Y.-L., Trahair, N.S., 1999. In-buckling and design of steel arches. Journal of Structural Engineering ASCE 125 (11), 1291–1298.

Rajasekaran, S., Padmanabhan, S., 1989. Equations of curved beams. Journal of Engineering Mechanics ASCE 115 (5), 1094–1111.

Schreyer, H.L., Masur, E.F., 1966. Buckling of shallow arches. Journal of the Engineering Mechanics Division ASCE 92 (EM4), 1–17.

Simitses, G.J., 1976. An introduction to the elastic stability of structures. Prentice-Hall, Englewood Cliffs, New Jersey.

Stolarski, H., Belytschko, T., 1982. Membrane locking and reduced integration for curved elements. Journal of Applied Mechanics Transactions ASME 49 (1), 172–176.

Timoshenko, S., Gere, J.M., 1961. Theory of Elastic Stability. McGraw-Hill, New York.

Trahair, N.S., Bradford, M.A., 1998. The Behaviour and Design of Steel Structures to AS4100, third Australian edition. E&FN Spon, London.

Vlasov, V.Z., 1961. Thin-walled Elastic Beams, second ed. Israel Program for Scientific Translation, Jerusalem.

Wen, R.K., Suhendro, B., 1991. Nonlinear curved-beam element for arch structures. Journal of Structural Engineering ASCE 117 (11), 599–612.